Biosynthesis of a major lipofuscin fluorophore in mice and humans with *ABCR*-mediated retinal and macular degeneration

Nathan L. Mata, Jian Weng, and Gabriel H. Travis*

Center for Basic Neuroscience and Department of Psychiatry, University of Texas Southwestern Medical Center, Dallas, TX 75235-9111

Communicated by David L. Garbers, University of Texas Southwestern Medical Center, Dallas, TX, March 13, 2000 (received for review December 2, 1999)

Increased accumulation of lipofuscin in cells of the retinal pigment epithelium (RPE) is seen in several forms of macular degeneration, a common cause of blindness in humans. A major fluorophore of lipofuscin is the toxic *bis*-retinoid, *N*-retinylidene-*N*-retinylethanolamine (A2E). Previously, we generated mice with a knockout mutation in the *abcr* gene. This gene encodes rim protein (RmP), an ATP-binding cassette transporter in rod outer segments. Mice lacking RmP accumulate A2E in RPE cells at a greatly increased rate over controls. Here, we identify three precursors of A2E in ocular tissues from *abcr*−/− mice and humans with *ABCR*-mediated recessive macular degenerations. Our results corroborate the scheme proposed by C. A. Parish, M. Hashimoto, K. Nakanishi, J. Dillon & J. Sparrow [*Proc. Natl. Acad. Sci. USA* (1998) 95, 14609–14613], for the biosynthesis of A2E: (*i*) condensation of all-*trans*-retinaldehyde (all-*trans*-RAL) with phosphatidylethanolamine to form a Schiff base; (*ii*) condensation of the amine product with a second all-*trans*-RAL to form a *bis*-retinoid; (*iii*) oxidation to yield a pyridinium salt; and (*iv*) hydrolysis of the phosphate ester to yield A2E. The latter two reactions probably occur within RPE phagolysosomes. As predicted by this model, formation of A2E was completely inhibited when *abcr*−/− mice were raised in total darkness. Also, once formed, A2E was not eliminated by the RPE. These data suggest that humans with retinal or macular degeneration caused by loss of RmP function may slow progression of their disease by limiting exposure to light. The precursors of A2E identified in this study may represent pharmacological targets for the treatment of *ABCR*-mediated macular degeneration.

Age-related macular degeneration (AMD) is a common cause of blindness in the elderly (1). It is characterized by the accumulation of fluorescent extracellular deposits called drusen and fluorescent lipofuscin granules in cells of the retinal pigment epithelium (RPE) (2–5). Lipofuscin accumulation in the RPE is also associated with Stargardt's disease (STGD1) and fundus flavimaculatus (FFM), recessive forms of macular degeneration that affect children (6, 7). These allelic disorders are caused by mutations in *ABCR* (8, 9). Heterozygous mutations in the *ABCR* gene may also predispose to AMD in a subset of cases (10, 11). *ABCR* encodes rim protein (RmP), an ATP-binding cassette transporter located in the rims of outer-segment discs (12–14). Rim protein (RmP) reconstituted in phospholipid vesicles containing phosphatidylethanolamine exhibits increased ATPase activity on addition of all-*trans*-retinaldehyde (RAL) (15, 16). Mice with a knockout mutation in the *abcr* gene have a complex ocular phenotype including elevated phosphatidylethanolamine in photoreceptor outer segments, elevated all-*trans*-RAL after light exposure, and accumulation of *N*-retinylidene-*N*-retinylethanolamine (A2E) in RPE cells (17). Based on these observations, it has been suggested that RmP may function as an outwardly directed flippase for phosphatidylethanolamine conjugated to all-*trans*-RAL (15–17).

Accumulation of A2E, the major fluorophore of lipofuscin (18, 19), is toxic to RPE cells (20–23). Parish *et al.* hypothesized that A2E forms by condensation of phosphatidylethanolamine with all-*trans*-RAL, followed by oxidation and hydrolysis of the phosphate ester (24). In this study, we corroborate this hypothesis by identifying three critical intermediates in the biosynthesis of A2E in ocular tissues from *abcr*−/− mice and humans with *ABCR*-mediated recessive macular degeneration.

Materials and Methods

Mouse Tissues. New-born wild-type and *abcr*−/− mice, both on an inbred 129-strain background, were raised under normal 12-h cyclic illumination (25–30 lux during light phase) or under total darkness in a ventilated cabinet for up to 18 weeks. Groups of six mice were analyzed per light condition. In a separate study, *abcr*−/− mice (hybrid strain 129 × BL6) were raised for 12 weeks under 12-h cyclic illumination, transferred to the dark, and groups of three mice were analyzed at 12, 16, 20, and 28 weeks. Mice were anesthetized with i.p. ketamine (200 mg/kg) plus xylazine (10 mg/kg) and killed by cervical dislocation. In experiments involving a photobleach, the pupils of anesthetized mice were dilated with 1.0% atropine sulfate, and the animals were exposed to 400 lux illumination in a Ganzfeld dome for 5 minutes, resulting in ≈45% bleaching of rhodopsin (17). Retinas were dissected from the posterior poles of each eye. The remaining RPE/eyecups were washed in PBS (pH 7.2). All dissections and tissue manipulations were performed on ice in dim red light.

Human Tissues. Sections of retina and overlying RPE were provided as postmortem specimens through the Histopathology Program of the Foundation Fighting Blindness (FFB). The FFM specimens were from a 62-year-old female with a clinical history of FFM (FFB no. 601), confirmed by published histopathological analysis (7). The postmortem interval (time of death to fixation) was 4.5 h. The STGD1 specimens were from a 73-year-old male with a clinical history of STGD1 (FFB no. 219). The postmortem interval was ≈12 h. Seven normal human retina and RPE specimens from patients with no retinal pathology were provided by Ann Milam, University of Pennsylvania, Philadelphia. Ages ranged from 71 to 85 yr ($\bar{x}$ = 77 yr). Postmortem intervals ranged from 3 to 16 h ($\bar{x}$ = 6.9 yr). All tissues were fixed in 4% paraformaldehyde plus 0.5% glutaraldehyde and stored in 2% paraformaldehyde. For each specimen, 0.5 × 0.5 cm sections from the perimacular region of the retina and overlying RPE

Abbreviations: RPE, retinal pigment epithelium; A2E, *N*-retinylidene-*N*-retinylethanolamine; A2PE-H_2, dihydro-*N*-retinylidene-*N*-retinylphosphatidylethanolamine; A2PE, *N*-retinylidene-*N*-retinylphosphatidylethanolamine; all-*trans*-RAL, all-*trans*-retinaldehyde; APE, *N*-retinylidene-phosphatidylethanolamine; FFM, fundus flavimaculatus; RmP, rim protein; RPE, retinal pigment epithelium; STGD1, recessive Stargardt's disease; MS, mass spectrometry.

*To whom reprint requests should be addressed at: Center for Basic Neuroscience, University of Texas Southwestern Medical Center, 5323 Harry Hines Boulevard, Dallas, TX 75235-9111. E-mail: travis@utsw.swmed.edu.

The publication costs of this article were defrayed in part by page charge payment. This article must therefore be hereby marked "*advertisement*" in accordance with 18 U.S.C. §1734 solely to indicate this fact.

Article published online before print: *Proc. Natl. Acad. Sci. USA*, 10.1073/pnas.130110497. Article and publication date are at www.pnas.org/cgi/doi/10.1073/pnas.130110497

Table 1. Phosphatidylethanolamine, all-*trans*-RAL, and APE in outer segments

Genotype	PE, pmol/eye	All-*trans*-RAL, pmol/eye	APE, pmol/eye	[H^+]APE, pmol/eye	% all-*trans*-RAL as APE
Wild type	17,200 ± 1,930	72.2 ± 1.87	13.8 ± 1.37	3.48 ± 1.31	24%
abcr−/−	33,300 ± 4,680	74.1 ± 2.87	40.8 ± 3.56	4.43 ± 0.59	61%

HPLC analysis for phosphatidylethanolamine (PE), all-*trans*-RAL, APE, and protonated APE ([H^+]APE) were performed on the same samples ($n = 3$) from wild-type and *abcr*−/− outer segments immediately after a 45% photobleach. All values are expressed as pmol per eye ± standard deviations. The last column shows the percent of total all-*trans*-RAL as APE (nonprotonated plus protonated) in wild-type and *abcr*−/− outer segments.

were analyzed after rinsing in Ringer's solution (pH 7.4) to remove fixative.

Tissue Preparation and Extraction. Mouse and human tissues were homogenized in 1 ml PBS. For analysis of mouse outer segments, dissected retinas were shaken on a vortex mixer in 8% Optiprep/Ringer's buffer and fractionated by centrifugation through an Optiprep step gradient according to the procedure of Tsang *et al.* (25). Collected outer segments were suspended in 1 ml PBS and homogenized. One milliliter of chloroform/methanol (2:1, vol/vol) was added to each homogenate. Phospholipids and chloroform-soluble fluorophores were extracted twice from the samples after addition of 4 ml of chloroform and 3 ml water. The pooled organic phases were dried under a stream of argon. Sample residues were resuspended in 200–400 μl of hexane and analyzed by HPLC.

Analysis of Phospholipids, Lipofuscin, and Retinoids. Sample extracts were analyzed by normal-phase HPLC by using a Hewlett–Packard 1100 liquid chromatograph with a photodiode array detector. Chromatography conditions were as previously described (17) using a silica column [Microsorb (Sigma) 5 μm Si, 250 × 4.6 mm] and the mobile phase: hexane/2-propanol/ethanol/25 mM potassium phosphate/acetic acid (485:376:100:40:0.275, vol/vol; pH 7.0). For dihydro-*N*-retinylidene-*N*-retinylphosphatidylethanolamine (A2PE-H_2) purification, the water content was reduced to 2.5% for better resolution of fatty acyl esters. Spectra for the eluted peaks were corrected by subtracting the nearest integrated baseline to remove solvent absorption. A2E, phosphatidylethanolamine, and all-*trans*-RAL were quantitated by comparing the sample peak area to a calibration curve constructed with authentic standards (18:0–22:6 for the phosphatidylethanolamine standard) (17). The yield of all-*trans*-RAL was lower than previously observed for total retina (17) because of losses incurred during the preparation of outer segments. In Table 1, *N*-retinylidene-phosphatidylethanolamine (APE) and protonated APE were quantitated by using published molar extinction coefficients (26).

Fatty Acid Analysis. Purified phospholipids were treated with 2% KOH and incubated at 100°C for 2 min (27). The mixtures were diluted in 1 ml water, acidified with concentrated HCL (10 μl/ml sample), and the free fatty acids (FFA) were partitioned into hexane (4 ml). The hexane extract was evaporated to dryness under argon gas, and the sample residue dissolved in 100 μl acetonitrile. FFAs were resolved by reverse-phase HPLC (Zorbax Eclipse XDB-C8, 5 μm, 4.6 × 150 mm) in acetonitrile/water/acetic acid (90:10:0.5, vol/vol) at 1 ml/min with a detection wavelength of 210 nm. Recovery was >90% as determined by equimolar recovery of 22:6 and 18:0 FFAs after saponification of authentic 22:6–18:0 phosphatidylethanolamine.

Mass Spectrometry (MS). Fast atom bombardment (FAB) MS was performed in a glycerol matrix by using a Micromass Quattro II triple quadrapole mass spectrometer (Manchester, U.K.) on samples purified by HPLC. Samples were dissolved in methanol/chloroform (2:1) + 1% acetic acid. Samples were continuously introduced into the source at a rate of 5 μl/min with an infusion pump. Masses were established in positive-ion mode. The FAB data were confirmed by electrospray MS (ESI) using the same instrument equipped with the manufacturer's standard electrospray source. FAB and ESI spectra were acquired every 5 seconds over an m/z range of 50–1050.

Conversion of A2PE-H_2 to A2E *in Vitro*. A2PE-H_2 was extracted from outer segments of *abcr*−/− mice and purified by HPLC as described above (2.5% water content; flow, 0.75 ml/min). The purified sample in phospholipid mobile phase was evaporated to dryness under a stream of argon and dissolved in 100 μl of phospholipid mobile phase in equilibrium with room air. One microliter of cold 10 N HCl was added (final concentration 100 mN). Aliquots were incubated for 5 min at 25°C or for longer periods at −20°C and analyzed by normal-phase HPLC. To test the role of an oxidizing environment on conversion of A2PE-H_2 to *N*-retinylidene-*N*-retinylphosphatidylethanolamine (A2PE) and A2E, purified A2PE-H_2 from 11-month *abcr*−/− retinas was suspended in phospholipid mobile phase. One aliquot was treated with 100 mN HCl and another with 100 mN HCl plus 2 mM DTT. After incubation as above, samples were analyzed by normal-phase HPLC.

Results

Increased APE in *abcr*−/− Outer Segments After Light Exposure. To begin our search for the precursors of A2E, we performed HPLC analysis on outer-segment extracts from wild-type and *abcr*−/− mice after a ≈45% photobleach. Although the levels of all-*trans*-RAL were similar between wild-type and *abcr*−/− outer segments, a significantly greater fraction of the all-*trans*-RAL in *abcr*−/− was present as APE (26, 28) (Table 1). The ratio of protonated to unprotonated APE was also different in wild-type and *abcr*−/− outer segments (Table 1). Similar ratios of protonated to unprotonated APE were observed when tissue samples were homogenized directly in chloroform/methanol, suggesting that the extraction buffer had no effect on the protonation state of APE.

A2PE-H_2 in Outer Segments and RPE of *abcr*−/− Mice. The presence of elevated APE in *abcr*−/− outer segments suggests that a second condensation with all-*trans*-RAL may occur to yield a *bis*-retinoid conjugate of phosphatidylethanolamine. We sought to identify molecules of this type by analyzing phospholipid extracts from 12-week-old wild-type and *abcr*−/− outer segments and RPE. An abundant molecular species with absorption maxima (λ_{max}) at 205 and 500 nm was identified in *abcr*−/− outer segments and RPE but was undetectable in wild-type tissues (Fig. 1). We named this species A2PE-H_2. A2PE-H_2 was undetectable in samples of *abcr*−/− rest of retina (depleted of outer segments), suggesting that in retina, A2PE-H_2 is located exclusively in outer segments. Moreover, A2PE-H_2 accumulated dramatically with advancing age (Fig. 1 *B* and *D*). The presence of multiple peaks in the A2PE-H_2 fractions is due to heterogeneity of the associated fatty acyl esters, as discussed below.

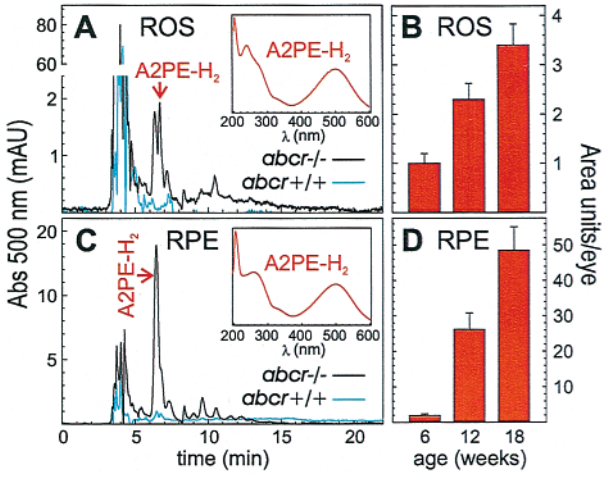

Fig. 1. HPLC analysis showing A2PE-H_2 in rod outer segment (ROS) and RPE. (*A*) Chromatogram of phospholipid extracts from 12-week-old *abcr*+/+ (light blue tracing) and *abcr*−/− (black tracing) ROS. Detection wavelength is 500 nm. *Inset* shows absorption spectrum of A2PE-H_2 peak fraction, indicated by red arrow. (*B*) Histogram showing levels of A2PE-H_2 in ROS from *abcr*−/− mice at the indicated ages in area units per eye. Error bars show standard deviations. (*C*) Chromatogram of phospholipid extracts from 12-week-old *abcr*+/+ (light blue tracing) and *abcr*−/− (black tracing) RPE. Detection wavelength is 500 nm. *Inset* shows absorption spectrum of the A2PE-H_2 peak fraction, indicated by red arrow. (*D*) Histogram showing the relative levels of A2PE-H_2 in RPE from *abcr*−/− mice at the indicated ages in area units per eye, ± standard deviations. Note that A2PE-H_2 is exclusively present in ROS and RPE from *abcr*−/− mice.

Conversion of A2PE-H_2 to A2E *in Vitro* on Acidification. If A2PE-H_2 represents an A2E precursor, it should be converted to A2E under *in vitro* conditions that simulate the acidic and oxidizing environment of RPE phagolysosomes. Samples of A2PE-H_2 purified from *abcr*−/− outer segments were incubated in phospholipid mobile phase containing 100 mN HCl prior to HPLC. After 5-minute incubation, a second molecular species appeared with different chromatographic properties and a visible-light λ_{max} of 430 nm, similar to A2E (Fig. 2*B*). Incubation of A2PE-H_2 overnight in the same solution resulted in the disappearance of both A2PE-H_2 and A2PE and the appearance of A2E plus phosphatidic acid (Fig. 2*C*). Quantitation of A2E and phosphatidic acid at the appropriate λ_{max} values yielded a molar ratio of ≈1:1 for these products. We confirmed our identification of the A2E formed after acid treatment of A2PE-H_2 by MS. This resulted in a major molecular-ion (m/z) peak of 592.3 (Fig. 2*D*), in good agreement with the calculated molecular mass of 592.45 for A2E ($C_{42}H_{58}ON$). We confirmed our identification of the phosphatidic acid by TLC and HPLC (not shown). With modification of the mobile phase, A2PE-H_2 could be separated into three chromatographic peaks (not shown). Fatty acid analysis on these separated peak fractions showed distinct fatty acid compositions, indicating different fatty acyl esters of A2PE-H_2. The major peak fraction of A2PE-H_2 from outer segments contained equimolar quantities of stearic (18:0) and docosahexanoic (22:6) acid, identical to the phosphatidic-acid product following acid incubation.

To test the dependence on an oxidizing environment on the conversion of A2PE-H_2 to A2PE and A2E, we added 2 mM DTT to purified A2PE-H_2 in the phospholipid mobile phase. The

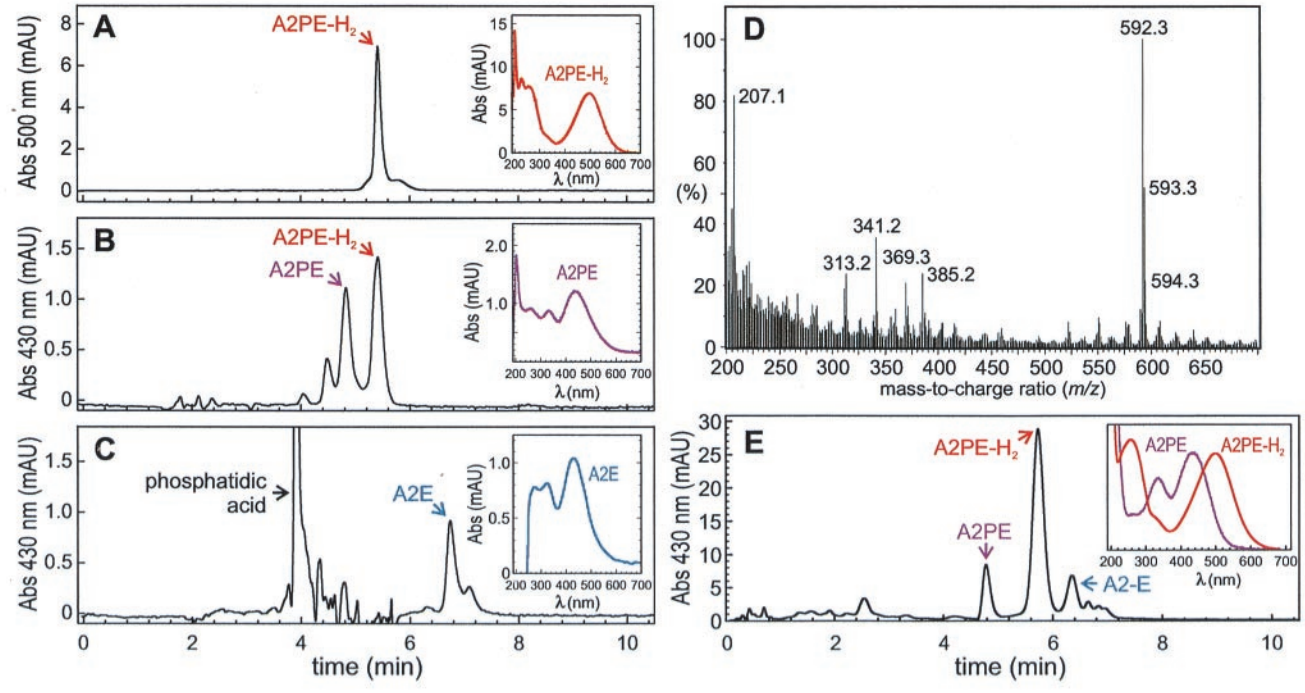

Fig. 2. HPLC analysis showing the A2PE intermediate in the formation of A2E. (*A*) Chromatogram of A2PE-H_2 purified from 11-month *abcr*−/− outer segments. Detection wavelength is 500 nm. *Inset* shows spectrum of the A2PE-H_2 peak, labeled with the red arrow. (*B*) Chromatogram of A2PE-H_2 fraction from *A* after 5 min incubation in HCl. Detection wavelength is 430 nm. The A2PE-H_2 peak is labeled with the red arrow. *Inset* shows spectrum of the A2PE peak, labeled with the purple arrow. (*C*) Chromatogram of A2PE-H_2 fraction from *A* after overnight incubation in HCl. Detection wavelength is 430 nm. The phosphatidic acid peak is labeled with the black arrow. *Inset* shows spectrum for the A2E peak, labeled with the blue arrow. Note the disappearance of A2PE-H_2 and A2PE and the appearance of phosphatidic acid and A2E. (*D*) Mass spectrum of A2E fraction from *C*. Note the major molecular-ion species with a m/z ratio of 592.3. The additional labeled peaks were also present in a sample containing only solvent. (*E*) Chromatogram of phospholipid extract from 6-month-old *abcr*−/− RPE. Detection wavelength is 430 nm. *Inset* shows spectra for the A2PE peak, labeled with the purple arrow, and A2PE-H_2 peak, labeled with the red arrow.

.

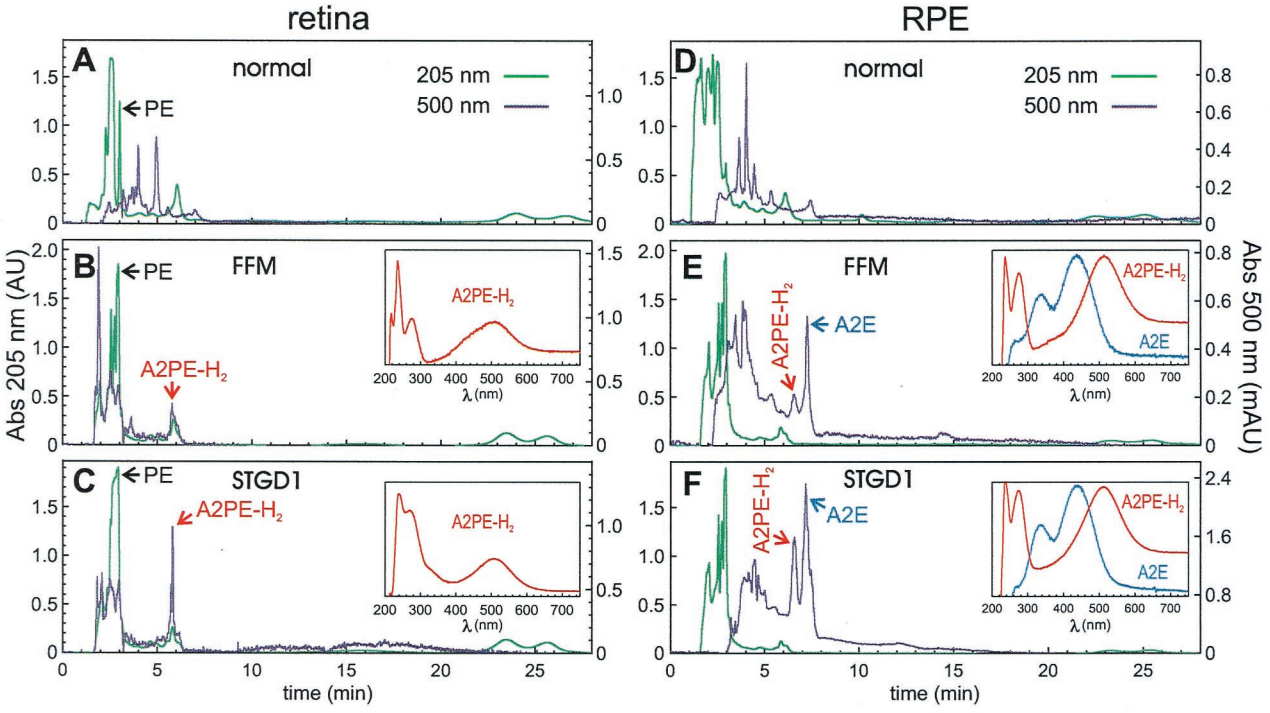

Fig. 3. HPLC analysis of phospholipid extracts from human retina and RPE showing phosphatidylethanolamine, A2PE-H_2, and A2E accumulation. *A* and *D* show analysis of retina and RPE, respectively, from a 71-year-old female with no retinal pathology as a representative control. *B* and *E* show analysis of retina and RPE, respectively, from a 62-year-old female with FFM. *C* and *F* show analysis of retina and RPE, respectively, from a 73-year-old male with STGD1. Chromatograms are shown at detection wavelengths of 500 (dark purple tracing) and 205 nm (green tracing) to display retinoid-conjugate and phospholipid absorption, respectively. For *A–F*, the 205-nm scale (*Left*) is in absorption units (AU), and the 500-nm scale (*Right*) is in milliabsorption units (mAU). Peaks corresponding to phosphatidylethanolamine (PE) in the retina samples are labeled with the black arrows. *Insets* show absorption spectra for the labeled A2PE-H_2 (red arrow) and A2E (blue arrow) peaks.

presence of DTT completely suppressed formation of both A2PE and A2E. However, similar amounts of phosphatidic acid were formed plus or minus DTT, indicating that acid hydrolysis of the phosphate ester does not depend on an oxidizing environment. In phospholipid mobile phase without added HCl, A2PE-H_2 was slowly converted to A2PE over approximately 1 month at −20°C. Thus, oxidation of A2PE-H_2 is strongly accelerated by acid. Finally, we analyzed a phospholipid extract of RPE from a 6-month *abcr*−/− mouse without prior acid treatment. Both A2PE-H_2 and A2PE were present (Fig. 2*E*), indicating that A2PE is a naturally occurring intermediate in the formation of A2E and not an artifact of acid treatment *in vitro*.

A2E and A2PE-H_2 in RPE from Humans with FFM and STGD1. To test the validity of the *abcr*−/− mouse as a model for *ABCR*-mediated recessive macular degeneration, we analyzed samples of postmortem retina and overlying RPE from the perimacular region of patients with FFM and STGD1, and seven human controls. Representative chromatograms are shown in Fig. 3. The levels of phosphatidylethanolamine were 22 and 30 μmol per 0.5 × 0.5 cm section of retina from the FFM and STGD1 patients, respectively, and 10.3 ± 1.79 (standard deviation) μmol per section of retina from the human controls. The levels of A2E were 33 and 61 pmol per 0.5 × 0.5 cm section of RPE from the FFM and STGD1 patients, respectively, and 5.30 ± 2.96 pmol per section of RPE from the human controls. A2PE-H_2 was present in both retina and RPE from the patient samples but undetectable in the controls (Fig. 3).

A2E in the RPE of Mice Reared Under Cyclic Light vs. Total Darkness. Previously, we observed significant accumulation of A2E in the RPE of *abcr*−/− mice (17). To test the dependence of this process on light-exposure history, we compared the levels of A2E in RPE from mice raised under cyclic light or total darkness. At 18 weeks under cyclic light, the levels of A2E in *abcr*−/− mutants were dramatically higher than those of wild-type mice (25.7 ± 2.60 vs. 1.98 ± 0.53 pmol/eye) (Fig. 4 *A* and *B*). In contrast, the levels of A2E were similar between 18-week-old wild-type and *abcr*−/− mice raised in total darkness (1.28 ± 2.60 and 1.89 ± 0.62 pmol/eye, respectively). In a separate study, a group of *abcr*−/− mice were raised for 12 weeks under cyclic light and transferred to total darkness. After transfer, no significant change in A2E levels was observed for up to 16 weeks in darkness (Fig. 4*C*). A2E was present only in RPE and was undetectable in retina or isolated outer segments under all conditions. Together, these data indicate that A2E accumulation in *abcr*−/− mice is strongly light dependent and that once formed, A2E is not removed by the RPE.

Discussion

Similar to humans with *ABCR*-mediated macular degenerations, *abcr*−/− knockout mice accumulate lipofuscin in cells of the RPE. In this study, we identified three precursors of A2E, the major fluorophore of lipofuscin. APE is the Schiff-base conjugate of phosphatidylethanolamine and all-*trans*-RAL (26, 28). A2PE-H_2 and A2PE were proposed as intermediates in the synthesis of A2E (24) but have not been previously identified.

Immediately after light exposure, we observed significantly elevated APE in *abcr*−/− compared with wild-type outer segments (Table 1). This difference is probably due to increased phosphatidylethanolamine in the mutants, because the levels of all-*trans*-RAL were similar in mice of both genotypes (Table 1). Most of the excess APE in *abcr*−/− outer segments was

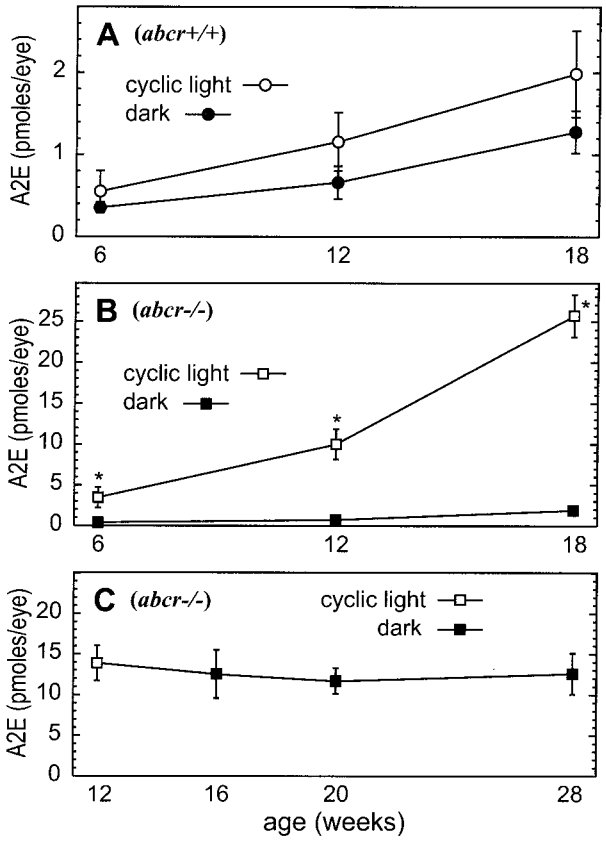

Fig. 4. A2E in RPE from mice raised under different light conditions. Data expressed in pmol A2E per eye from mice of the indicated ages. (*A*) Wild-type (*abcr*+/+) mice raised under cyclic light (open circles) or in total darkness (filled circles). (*B*) *abcr*−/− mutant mice raised under cyclic light (open circles) or in total darkness (filled circles). (*C*) *abcr*−/− mutant mice raised for 12 weeks under cyclic light and transferred to total darkness until reaching the indicated ages. Error bars show standard deviations. * indicates a significant difference between data points by Student's *t* test ($P < 0.05$).

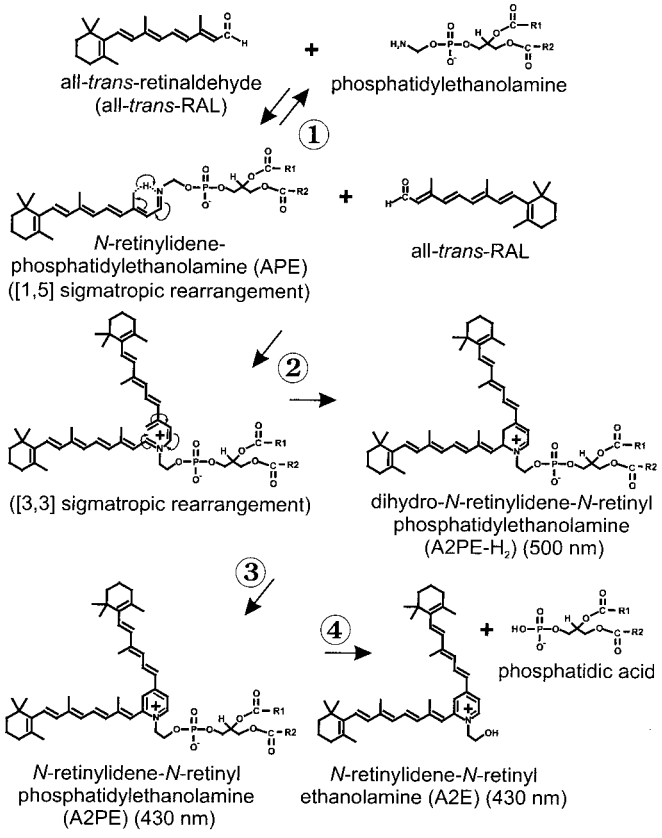

Fig. 5. Hypothetical biosynthetic pathway for A2E in mice and humans lacking the RmP transporter. This model is based on the proposed scheme for A2E biogenesis by Parish *et al.* (24). In outer segments after a photobleach, phosphatidylethanolamine and all-*trans*-RAL are transiently in equilibrium with APE (reaction 1). After a (1, 5) sigmatropic rearrangement, the resulting secondary amine may condense with another molecule of all-*trans*-RAL. Subsequent (3, 3) sigmatropic rearrangement of the *bis*-retinoid product results in the formation of A2PE-H_2 (reaction 2), an irreversible step at neutral pH. Oxidation of A2PE-H_2 to A2PE (reaction 3) occurs within RPE phagolysosomes and is accompanied by a shift in the visible λ_{max} from 500 to 430 nm. This blue shift is expected, because the two tetraene side chains are oriented *meta* on the pyridinium ring, hence resonance delocalization occurs at a higher energy in the oxidized form because of loss of aromaticity. Finally, A2E is formed within RPE phagolysosomes on acid hydrolysis of the phosphate ester and release of phosphatidic acid (reaction 4).

unprotonated (Table 1), possibly indicating higher intradiscal pH immediately after a photobleach. This form, in contrast to protonated APE, is capable of sigmatropic rearrangement and subsequent condensation with a second molecule of all-*trans*-RAL to yield A2PE-H_2 (Fig. 5). A2PE-H_2 was abundantly present in *abcr*−/− outer segments and RPE and accumulated dramatically with age (Fig. 1). Unexpectedly, A2PE-H_2 was undetectable in wild-type outer segments despite the presence, albeit at a lower level, of APE. This suggests that clearance of APE in wild-type outer segments is significantly faster than the rate of A2PE-H_2 formation.

Brief incubation of A2PE-H_2 in HCl resulted in the appearance of a second chromatographic peak with different spectral properties, which we named A2PE (Fig. 2). Overnight incubation in HCl resulted in the complete conversion of A2PE-H_2 to A2E and phosphatidic acid. Incubation in similar medium with the addition of a mild reducing agent completely suppressed formation of A2PE and A2E but had no effect on the release of phosphatidic acid. Thus, oxidation of the pyridinium ring and hydrolysis of the phosphate ester represent independent steps in the formation of A2E. A2PE and A2E both had a λ_{max} of 430 nm. This was expected, because these molecules have identical resonating structures (Fig. 5). Loss of the phospholipid moiety in A2E is evident spectrally by loss of the 205-nm absorption peak (Fig. 2 *B* and *C Insets*). A2PE-H_2, which lacks the third double bond of the pyridinium ring, has a visible λ_{max} of 500 nm. We confirmed our identification of the A2E and phosphatidic-acid products after incubation in HCl by MS and HPLC, respectively. The major form of A2PE-H_2 had the identical fatty acid composition as the phosphatidic-acid product of its hydrolysis and the predominant form of phosphatidylethanolamine in outer segments (29). These data suggest that A2PE-H_2 is the source of phosphatidic acid after incubation in HCl and that phosphatidylethanolamine from outer segments is the starting material for A2PE-H_2 formation. The stability of A2PE-H_2 in a nonoxidizing environment suggests that reaction 2 in Fig. 5 is effectively irreversible. A2PE-H_2 was present in both retina and RPE of *abcr*−/− mice. A2PE and A2E, however, were exclusively present in RPE. These observations suggest that the final two reactions in Fig. 5 occur only within the oxidizing and acidic environment of RPE phagolysosomes.

The biochemical abnormalities in outer segments and RPE from *abcr*−/− mice were similar to those observed in postmortem tissues from two patients with STGD1 and FFM. In particular, phosphatidylethanolamine was 2- to 3-fold more abundant in retina, and A2E 6- to 12-fold more abundant in RPE

from patients vs. controls. A2PE-H_2 was abundantly present in retina and RPE from both patients but was undetectable in control tissues (Fig. 3). The specific molecular defects in the patients presented here have not yet been defined. However, because FFM and STGD1 are both recessive diseases caused by mutations in *ABCR* (8, 9, 30), these patients presumably have partial or complete loss of RmP function. The similarity of phenotypes between *abcr*$-/-$ mice and humans with *ABCR*-mediated diseases was surprising, given that FFM and STGD1 are predominantly macular degenerations and that mouse retina does not contain a macula. In humans, greater vulnerability of the macula to the *ABCR*-mediated disease process may be secondary to the higher ratio of outer segments to RPE cells in this area (31).

One prediction of the pathway proposed in Fig. 5 is that A2E accumulation should depend on the availability of all-*trans*-RAL and hence on light exposure. To test this hypothesis, we blocked any increase above basal levels of all-*trans*-RAL by raising *abcr*$-/-$ mice under total darkness. The level of A2E in these animals was approximately equal to that of wild-type mice (Fig. 4 *A* and *B*). Thus, the increased formation of A2E in *abcr*$-/-$ mice is completely light dependent, which supports the proposed pathway. Interestingly, when mice raised under cyclic light for 12 weeks were transferred to the dark, no reduction in the level of A2E was observed, even after 16 weeks in total darkness (Fig. 4*C*). These data indicate that A2E is not cleared by the RPE in *abcr*$-/-$ mutants, in contrast to the transient accumulation of lipofuscin reported in rats after intravitreal leupeptin injection (32). The observed inhibition of A2E accumulation in *abcr*$-/-$ mice raised under total darkness suggests that limiting light exposure may reduce the rate of disease progression in humans with recessive *ABCR*-mediated diseases. Although the mechanism of A2PE-H_2 formation undoubtedly varies with genetic etiology, the final pathway of A2E accumulation may be similar in other forms of lipofuscin-mediated macular or retinal degeneration. Pharmacologic inhibition of one or more steps in the A2E synthetic pathway may thus be an effective treatment strategy for other macular degenerations associated with lipofuscin accumulation.

The authors gratefully acknowledge Bikash Pramanik and Roxana Radu for their outstanding technical contributions, Sassan Azarian and Wojciech Kedzierski for their useful comments on the manuscript, Michael Biewer and Patrick Harran for their valuable insights into the organic chemistry, and Ann Milam and the Foundation Fighting Blindness (FFB) for providing human donor tissues. This work was supported by grants from the National Eye Institute, the FFB, and the Macula Vision Research Foundation.

1. Bressler, N. M., Bressler, S. B. & Fine, S. L. (1988) *Surv. Ophthalmol.* **32,** 375–413.
2. Bressler, N. M., Silva, J. C., Bressler, S. B., Fine, S. L. & Green, W. R. (1994) *Retina* **14,** 130–142.
3. Kliffen, M., van der Schaft, T. L., Mooy, C. M. & de Jong, P. T. (1997) *Microsc. Res. Tech.* **36,** 106–122.
4. Sarks, S. H., Arnold, J. J., Killingsworth, M. C. & Sarks, J. P. (1999) *Br. J. Ophthalmol.* **83,** 358–368.
5. Delori, F. C., Fleckner, M. R., Goger, D. G., Weiter, J. J. & Dorey, C. K. (2000) *Invest. Ophthalmol. Visual Sci.* **41,** 496–504.
6. Eagle, R. C., Jr., Lucier, A. C., Bernardino, V. B., Jr. & Yanoff, M. (1980) *Ophthalmology* **87,** 1189–1200.
7. Birnbach, C. D., Jarvelainen, M., Possin, D. E. & Milam, A. H. (1994) *Ophthalmology* **101,** 1211–1219.
8. Allikmets, R., Singh, N., Sun, H., Shroyer, N. F., Hutchinson, A., Chidambaram, A., Gerrard, B., Baird, L., Stauffer, D., Peiffer, A., *et al*. (1997) *Nat. Genet.* **15,** 236–246.
9. Rozet, J. M., Gerber, S., Souied, E., Perrault, I., Chatelin, S., Ghazi, I., Leowski, C., Dufier, J. L., Munnich, A. & Kaplan, J. (1998) *Eur. J. Hum. Genet.* **6,** 291–295.
10. Allikmets, R., Shroyer, N. F., Singh, N., Seddon, J. M., Lewis, R. A., Bernstein, P. S., Peiffer, A., Zabriskie, N. A., Li, Y., Hutchinson, A., Dean, M., *et al.* (1997) *Science* **277,** 1805–1807.
11. Lewis, R. A., Shroyer, N. F., Singh, N., Allikmets, R., Hutchinson, A., Li, Y., Lupski, J. R., Leppert, M. & Dean, M. (1999) *Am. J. Hum. Genet.* **64,** 422–434.
12. Papermaster, D. S., Schneider, B. G., Zorn, M. A. & Kraehenbuhl, J. P. (1978) *J. Cell Biol.* **78,** 415–425.
13. Azarian, S. M. & Travis, G. H. (1997) *FEBS Lett.* **409,** 247–252.
14. Illing, M., Molday, L. L. & Molday, R. S. (1997) *J. Biol. Chem.* **272,** 10303–10310.
15. Sun, H., Molday, R. S. & Nathans, J. (1999) *J. Biol. Chem.* **274,** 8269–8281.
16. Sun, H. & Nathans, J. (2000) in *Methods Enzymol.*, ed. Palczewski, K. (Academic, San Diego), Vol. 315, pp. 879–897.
17. Weng, J., Mata, N. L., Azarian, S. M., Tzekov, R. T., Birch, D. G. & Travis, G. H. (1999) *Cell* **98,** 13–23.
18. Sakai, N., Decatur, J., Nakanishi, K. & Eldred, G. E. (1996) *J. Am. Chem. Soc.* **118,** 1559–1560.
19. Reinboth, J. J., Gautschi, K., Munz, K., Eldred, G. E. & Reme, C. E. (1997) *Exp. Eye Res.* **65,** 639–643.
20. Sundelin, S., Wihlmark, U., Nilsson, S. E. G. & Brunk, U. T. (1998) *Curr. Eye Res.* **17,** 851–857.
21. Holz, F. G., Schutt, F., Kopitz, J., Eldred, G. E., Kruse, F. E., Volcker, H. E. & Cantz, M. (1999) *Invest. Ophthalmol. Visual Sci.* **40,** 737–743.
22. Eldred, G. E. & Lasky, M. R. (1993) *Nature (London)* **361,** 724–726.
23. Sparrow, J. R., Parish, C. A., Hashimoto, M. & Nakanishi, K. (1999) *Invest. Ophthalmol. Visual Sci.* **40,** 2988–2995.
24. Parish, C. A., Hashimoto, M., Nakanishi, K., Dillon, J. & Sparrow, J. (1998) *Proc. Natl. Acad. Sci. USA* **95,** 14609–14613.
25. Tsang, S. H., Burns, M. E., Calvert, P. D., Gouras, P., Baylor, D. A., Goff, S. P. & Arshavsky, V. Y. (1998) *Science* **282,** 117–121.
26. Anderson, R. E. & Maude, M. B. (1970) *Biochemistry* **9,** 3624–3628.
27. DeMar, J. C., Jr., Wensel, T. G. & Anderson, R. E. (1996) *J. Biol. Chem.* **271,** 5007–5016.
28. Poincelot, R. P., Millar, P. G., Kimbel, R. L., Jr. & Abrahamson, E. W. (1969) *Nature (London)* **221,** 256–257.
29. Stinson, A. M., Wiegand, R. D. & Anderson, R. E. (1991) *Exp. Eye Res.* **52,** 213–218.
30. Stone, E. M., Webster, A. R., Vandenburgh, K., Streb, L. M., Hockey, R. R., Lotery, A. J. & Sheffield, V. C. (1998) *Nat. Genet.* **20,** 328–329.
31. Jonas, J. B., Schneider, U. & Naumann, G. O. (1992) *Graefes Arch. Clin. Exp. Ophthalmol.* **230,** 505–510.
32. Katz, M. L., Rice, L. M. & Gao, C. L. (1999) *Invest. Ophthalmol. Visual Sci.* **40,** 175–181.